300-fold higher neuro- and immunotoxicity from low-redox transformation of carbamazepine

Tom M. Nolte [a,b]

[a] *Department of Environmental Science, Institute for Water and Wetland Research, Radboud, University Nijmegen, 6500 GL Nijmegen, the Netherlands*
[b] *Eidgenössische Technische Hochschule (ETH) Zurich, Laboratory of Inorganic Chemistry, Vladimir-Prelog-Weg 1, 8093 Zurich, Switzerland*

ARTICLE INFO

ABSTRACT

Current challenges in (eco)toxicology are in understanding the transformation of (reactive) substances, and how transformation affects toxic modes of action. Empirical assessment of transformation products of, practically an infinite number of substances, via experimentation, is impossible. Predicting transformation products for (benchmarking) compounds from conditions, facilitates risk analyses. This study applied calculus to predict transformation products of an important environmental and medicinal/toxicological marker, carbamazepine. As radicals are ubiquitous in humans and the environment, we looked into radical-mediated transformations of carbamazepine as a benchmark. We calculated proportions of their speciation states as function of redox conditions, which we took as pH and O_2 concentration, describing transformation via covalent and ionic interactions. Formation of ring-contracted products with neuro-immunological activity is thermodynamically favored under anaerobic conditions and at low pH. Experimentally observed product distributions and toxicities reflect that pattern. Our predictive method may support toxicity predictions for other substances and conditions 'similar' to the current case study via interpolation. This paves the way for a more coherent, effective and easier risk assessment of transformation products.

1. Introduction

Challenges in (eco)toxicology are in understanding transformation of reactive substances, and how this affects toxic modes of action. Thereby, transformation products and intermediates in degradation gain increasing attention. Empirical assessment of transformation products of, potentially 10^{24} substances [1–3], via experimentation, is impossible. We need indicator compounds from which we can more efficiently asses. One such compounds may be the antiepileptic drug carbamazepine (CMZ), which blocks calcium channels to inhibit neurotransmission [4]. With up to 200 million patients receiving treatment worldwide [5,6], metabolites of CMZ would cause substantial amounts of side effects even if the corresponding probability is low. The metabolite acridine is observed in plasma of patients suffering from gastrointestinal side effects of CMZ [7]: nausea, vomiting, diarrhea, heartburn, constipation, dysphagia and stomachache [8].

(Bio)chemical transformations of CMZ occur in the human body as well as in waste- and surface water: pharmacoactive or genotoxic CMZ metabolites were identified both in humans and wastewaters [9]. CMZ is a marker for risk assessment (RA) [5,10] and water management [11, 12]. Environmental contamination is caused by excretion of CMZ and its

metabolites, or improper use and disposal. CMZ is detected in wastewater effluents and hence is only partly removed by conventional biological treatment. Environmentally persistent pharmaceuticals like CMZ (resistant to biodegradation) are detected in surface waters around the world, with risks to human and environmental health. This necessitates removal like (in)direct photolysis [13], but UV-treatment of wastewater and photolysis in natural waters produces CMZ transformation products [14].

The immune system defends against bacteria, viruses and other bodily invaders. Immunotoxic substances affect immune cells, cytokines, antibody production, etc., causing increased susceptibility of disease. In patients, 9-acridine carboxaldehyde may cause adverse reactions [15]. Whereas CMZ itself had no effect, 100 μM 9-acridine carboxaldehyde killed 40% of lymphocytes, and 0.08–1.0 μM 9-acridine carboxyaldehyde altered immune cell function [16]. Binding of 9-acridine carboxaldehyde to neutrophils was 200 times more efficient that of CMZ, Table 1, suggesting that the aldehyde is responsible as a reactive intermediate. Its binding with nucleophiles occurs with primary amines (butylamine, N-α-acetyl lysine), forming (neurotoxic, cyclic) imines and indole alkaloids [15,17,18]. These products block relevant (neuro-immunologic lymphocytic) acetylcholine receptors [19–22], Fig. 1. CMZ

Table 1

Toxicity of carbamazepine and its transformation products, as highlighted in Fig. 1;2. The aldehyde and imine are > 100× as toxic.

	Carbamazepine	Dioxoquinazolinyl-benzoic acid‡	Acridine-carboxaldehyde⁎⁎	Indolylidene-hexadienimine⫽
Fish 96-hr LC$_{50}$, mg/L+	41 [28]	193 [28]	3 [28]	0.4 [28]
Rat (oral) LD$_{50}$, mg/kg+	1957 [29,30]	2552 [29,30]†	80 [29–32]*	8¶
Neutrophil binding pmol/10⁶ cells	50 [15]	< 50‡	10000 [15]	-

+LD$_{50}$ = the concentration at which 50% of a population dies. *log-average for 10+ related acridines, †log-average for 3 related oxoquinazolines [33], ‡extrapolation of values in table, ‡2-(2,4-dioxoquinazolin-1-yl)benzoic acid ⁎⁎9-acridine-carboxaldehyde, ⫽(1E,6E)−6-(3H-indol-3-ylidene)-N-methylcyclohexa-2,4-dien-1-imine. ¶using regression in Fig. 7.
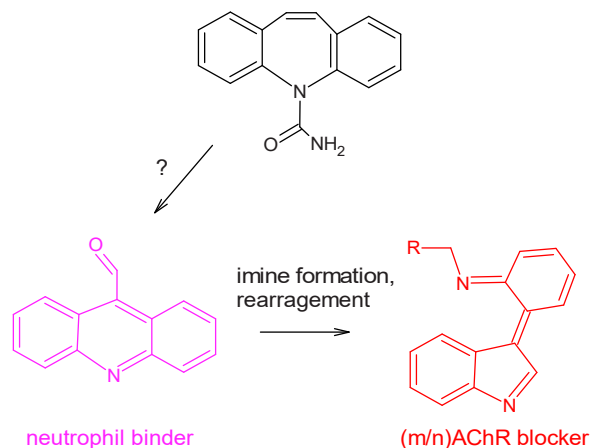

Fig. 1. Radical-instigated reactions with carbamazepine can produce toxic neutrophil binders (9-acridine carboxaldehyde) and acetylcholine esterase blockers (indolcyclohexadieneimine[1]). The step marked with "?" is central to our investigation. (m/n)AChR = nicotinic and muscarinic acetylcholine receptors.

(metabolites) associate with leukocyte antigen genotypes [23], immunological activity [24], bone marrow cancer [25], leukopenia [26], hypothyroidism [27] and toxidermia.

Ecotoxicity can increase with degradation [21]: (a mix of) transformation products was considerably more toxic than CMZ itself [14]. Toxicity increases if waste-, river or groundwater systems transform CMZ into a more recalcitrant metabolite [34]. Ring-contracted products (e.g., acridine and acridone) appear generally more cyto- and genotoxic to organisms and ecotoxic [35]; the metabolite 9-acridine carboxaldehyde is markedly more toxic to fish and rat than is its parent CMZ (Table 1). Among CMZ and its metabolites, acridine 9-carboxylic acid is particularly toxic to freshwater species [36]. While experiments empirically investigated CMZ product formation, factors in play are still not thoroughly understood. To elucidate and remediate toxicity of CMZ transformation products, we need to understand how these are formed, Fig. 1. Free-energy relationships showed that contraction of rings increases toxicity [37,38] by affecting redox status [39,40].

1.1. Transformation pathways

The main (hepatic) enzyme involved in metabolizing CMZ is Cytochrome P450, CYP3A4, producing carbamazepine-10,11-epoxide [41, 42]. Reaction with reactive oxygen species (ROS) or radicals transform CMZ and its epoxide. ROS/radicals are produced, for example, via immune function in the gut [43,44], catalytic conversion of H_2O_2 to HOCl by myeloperoxidasee in leukocytes [45,46], synaptic Ca^{2+}-signalled neurotransmission and plasticity [47,48], autooxidation of neurotransmitters [49] and reaction between Fe/thiols [50]. From this wealth of neuro-immunological, toxicological, metabolic and (UV-induced)

photocatalytic reactions in the human body and waste/surface waters [51], we presume that cation derivatives of CMZ are (indirectly) formed (e.g., elimination of H_2O by hydroxylated CMZ). Such cations are precursors to ring-contracted toxicants [52].

Redox status is key to elucidate transformation pathways [53] e.g., via free-energy relationships [54,55]. Oxygenation can accelerate ROS/radical production, improve mineralization [51] and (in)activate CMZ derivates. Transformation of CMZ into acridine is associated with anaerobic digestion (i.e., biogas production) [56]. The gut is mostly anaerobic [57] with anaerobic bacteria therein. Photocatalytic formation of acridine from CMZ increases ~3-fold from 306 to 66 μM O_2 (9.8–2.1 mg L^{-1}, at pH 3 and 10) [51]. Removal of CMZ and acridine was more efficient aerobically [51]. Effect of pH on solar degradation indicates involvement of protonation: CMZ removal increased ~49–61% between pH 7–9 [58]. While high pH can enhance photocatalytic degradation [51], low stomach pH (~2) might favor specific transformation pathways.

Aforementioned gives insight but precise influences on transformation remain unclear; quantitative data as function of pH/O_2 is sparse. Opting to facilitate RA based on redox properties, we considered transformations for CMZ. More detailed information on redox properties driving formation of toxic (CMZ) metabolites can improve RA and elucidate and moderate side effects. In this study, we quantified toxicity of transformation mixes via thermodynamic calculations involving pH/O_2. We hypothesized that toxicity varies according to different pH/O_2, and studied redox-dependent CMZ products via kinetics characterizing pH-dependent and (an)aerobic reactions. We developed calculus predicting formation of CMZ transformation products, which we tested with toxicity data. Results show significant variance in radical-induced CMZ toxicity which we interpreted by highlighting varying pH/O_2 during neuroimmune functioning, in the bloodstream, surface- and sediment porewater.

2. Methods

2.1. Toxic ratios

We evaluated toxicity of CMZ transformation products. We hypothesize the concentration of (non-)toxic transformation products to be a function of pH/O_2, and our investigation considers primary addition/elimination reactions as function of pH and O_2 concentration leading to steady-states. Like all reactions, additions are, in principle, reversible. We assume all follow-up reactions after equilibria to contribute equally between aerobic and anaerobic pathways (outlook section). We thereby test the relevance of primary equilibria for in situ toxicological potential. In other words, equilibrium constants K to characterize the relative likelihood of formation of toxic products. How K relates to detailed in situ product distributions we will not further discuss. We therefore formulate a ratio K_{tox} of toxic concentrations [59,60]:

$$K_{tox} = \frac{ring-contr.prods}{ring-open.prods} \tag{1}$$

The precise nature, behaviors and distributions of the activated state (s) of CMZ (derivatives) is multidimensional. Acknowledging the

_____
[1] (6E)−6-(3 H-indol-3-ylidene)cyclohexa-2,4-dien-1-imine

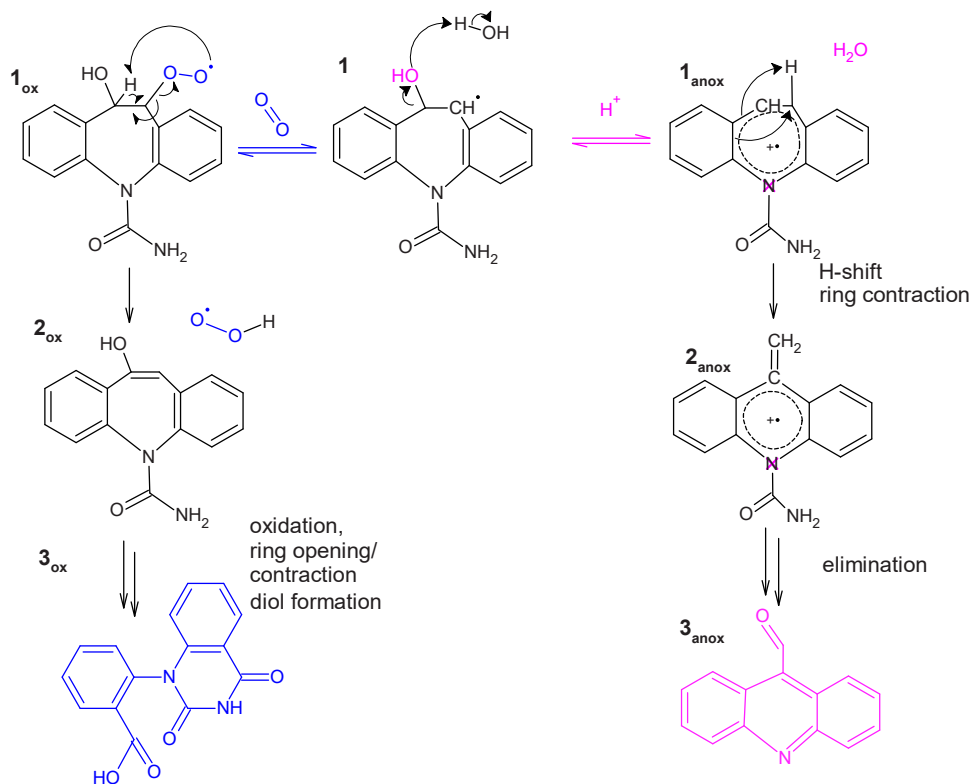

Fig. 2. Hypothesized radical-mediated degradation pathway for carbamazepine. Horizontal and vertical arrows are equilibration and follow-up reactions, resp. While H—abstraction has minor contribution [61], double bonds in heterocyclic rings are most vulnerable place for attack [62–64]. Cation formation facilitates ring contraction [52]. Depending on concentrations of O_2 and H^+, the pathway would result in different end products, with different toxicities. Elimination of water by the OH-adduct may be facilitated by H^+. We evaluated toxicity by calculating relative equilibrium concentrations of 1_{ox} ('non-toxic') versus 1_{anox} (leading to toxic ring contracted products) under varying concentration of O_2 and H^+.

importance of redox, we considered radical reactions and properties of CMZ that are representative indicators of a range of redox-mediated transformations involving CMZ (derivatives) in the body/nature. As authors report H^+-catalyzed elimination of H_2O by CMZ-OH, we presume a CMZ-OH$_2^+$ species exists, whatever its lifetime and nature may be. By considering radical reactions depicted in Fig. 2, we rewrite Eq.1 to:

$$K_{tox} = \frac{10^{-pH} \times \frac{K_{CMZ^{\bullet+}/CMZ-OH}}{1 \times 10^{14}} + \frac{K_{CMZ^{\bullet+}/CMZ-OH_2^+}}{55.5}}{[O_2] \times K_{CMZ-OH-O_2^\bullet/CMZ-OH^\bullet}} \quad (2)$$

We thereby express an equilibrium constant for addition in terms of adduct formation (K, in M^{-1}) and elimination (K, in M). For addition reactions: $A + B \rightleftharpoons C$, in our case A and C are CMZ-OH$^\bullet$, CMZ-OH-O$_2^\bullet$, CMZ-OH$_2^{\bullet+}$ and CMZ$^{\bullet+}$, depending on the reaction (Fig. 2). Entries for [B] are either [O_2], [OH^-] or [H^+]. We take the reactions of the order 1, meaning only 1 species participates, thus:

$$K_\rightarrow = \frac{[C]}{[A] \times [B]} \quad (3)$$

Wherein $K_\rightarrow = k_\rightarrow/k_\leftarrow$ is the equilibrium constant. Via variation in B (pH/pO$_2$) we study the effect of redox on the transformation pathway to specific intermediates and toxic products. Ring-opening (e.g., of structure 1) is not a significant pathway and not meditated by pH/O$_2$ (Section 3.4, Fig. 5A).

2.2. Calculating equilibrium constants

As values for K for O_2 addition for structure 1_{ox} affect the extent of ring opening (Fig. 2), we obtained it via thermochemical calculation and experiment. We similarly obtained values for rate constants K for

addition of OH^-/H_2O (1_{anox}):

$$K_\rightarrow = \frac{k_\rightarrow}{k_\leftarrow} \quad (4\text{ -}1)$$

wherein $k_\rightarrow$ and $k_\leftarrow$ are forward and backward rate constants. We evaluated calculated $k_\rightarrow$ and $k_\leftarrow$ by comparison to literature data. For calculating k we applied Arrhenius using activation energies $\Delta G^\ddagger$ (from literature) and $\Delta\Delta G^\ddagger$, obtained via linear-free-energy-relationships [65], e.g. for the forward reaction:

$$k_\rightarrow = A \cdot e^{\frac{-\Delta G^\ddagger_\rightarrow + \Delta\Delta G^\ddagger_\rightarrow}{R \cdot T}} \quad (4)$$

$$\Delta\Delta G^\ddagger_\rightarrow = \sigma_{PF}\Delta\Delta G_{PF} + \sigma_{CS}\Delta\Delta G_{CS}\frac{\lambda_M}{F_c} \quad (5)$$

We obtained free energies $\Delta\Delta G$ via frontier molecular orbitals (FMO) and thermodynamic cycle as described by the models by Nolte et al. (2), details in [65]. For example, $k_\rightarrow$ for reaction between the biradical O_2 and CMZ-OH$^\bullet$, we computed the charge transfer ("resonance") energy ΔG_{CS} as $1/(E_{LUMO(CMZ-OH-O2\bullet)}-E_{SOMO(CMZ-OH-O2\bullet)})$, and ΔG_{PF} as $1/(E_{SOMO(O2)}-E_{SOMO(CMZ-OH\bullet)})$ - ΔG_{CS}, where SOMO is the singly occupied molecular orbital. Fig. 2–2 visualizes the method based on orbital energies for addition of radicals onto imidazole:

2.3. Experimentation

We ascertained calculated k and K values via experiments. We prepared aqueous (Millipore-Q) solutions saturated with O_2/N_2O gas in Schlenk-tubes by repeated evacuated to 10mbar and refilled (minimum of 3 repeats) with the desired gas. Solutions were transferred from a gas-tight syringe (10 ml, Hamilton, SampleLock, Bonaduz,Switzerland) to

quartz cells (6 cm, Hellma, Müllheim, Germany) via a syringe pump. We performed pulse radiolysis experiments on a Febetron 705 (Titan Systems Corp. L-3 Comm., San Leandro, CA, USA) with optical detection (details in [67]). We pulse-irradiated solutions with < 50 ns of 2 MeV electrons, measuring doses using a thiocyanate dosimeter.

Irradiation of H_2O forms primary spur species with yields G(OH$^\bullet$) (molecules per 100 eV absorbed dose), pH 7, G(e_{aq}^-) and G(H$^\bullet$) of 2.7, 2.7 and 0.6, respectively, whereby G = 1 equals generation of 0.1036 mmol of a species per 1 J kg^{-1} absorbed energy [68–70]. Solutions were saturated with either N_2O (22 mM) to increase the OH$^\bullet$ yield, or mixtures of O_2/N_2O. The solvated electron, e_{aq}^-, reacts with N_2O to yield more OH$^\bullet$: $N_2O + e_{aq}^- + H_2O \rightarrow N_2 + OH^\bullet + OH^-$. Hence, a N_2O saturated condition yields G = 5.4 for OH$^\bullet$. Reaction of OH$^\bullet$ with an aromatic unit (top in Fig. 2) produces the hydroxycyclohexadienyl adduct of CMZ, i.e., CMZ-OH$^\bullet$. We studied varying concentrations and doses of O_2 and OH$^\bullet$ on kinetic traces.

3. Results and discussion

3.1. Toxic concentrations under varying pH/O_2

CMZ-OH$^\bullet$ can be in equilibrium with the O_2-adduct (CMZ-OH-$O_2^\bullet$), the cation (CMZ$^{\bullet+}$). Technically, CMZ-OH$_{open}^\bullet$ can form a ring-opened species, but this is unfavorable (Fig. 5A). We expect CMZ-OH-$O_2^\bullet$ to contribute least to toxicity, as it is the primary precursor to ring-opened products (Fig. 2). Increasing O_2 gives more ring-opened products via the formation of O_2-adducts, epoxide species, diols, etc. (Fig. 2). Conversely, decreasing pO_2 allows more ring-contracted product formation via e.g., radical cations. Experiments verify that low pH favor generating acrid (o/i)ne products. Varying pH/pO_2 would influence ratios of toxic products given in Table 1.

To quantify toxicity of the CMZ product mix, we calculated ratios of toxic over non-toxic products: using 4 values for $K_{H2Oelim}$, $K_{OH-elim}$, K_{O2add} and K_{open} and implementing O_2, H^+ and H_2O (55.5 M) concentrations, we obtained equilibrium 'toxic concentration ratios' K_{tox} (Eq. 2). Coming from a 'standard' or 'benchmarked' toxicity at pH= 7.5 and saturated O_2 (Fig. 3), removal of O_2 or lowering pH can maximally multiply toxicity by a factor 3 (to red entries). Conversely, toxicity might be reduced (maximally by a factor 30) by increasing O_2, but mostly by increasing pH (to green entries). These changes are the result of equilibrium concentrations of O_2-adducts and cations under varying pH/pO_2, driven by their affinity K values.

Values for equilibrium constants K are such that real-world variations in pH/pO_2 give rise to varying toxicities in physiological and environmental situations. In the bloodstream $[O_2]\sim4–10 \times 10^{-5}$ M [71] but lower under high altitude. Thus, CMZ use under high altitude may require stricter safety [72]: lower blood oxygen would deteriorate CMZ activity [73]. In the anaerobic stomach, the local pH~2 allows 3 times higher values of ring-contracted products via cations were
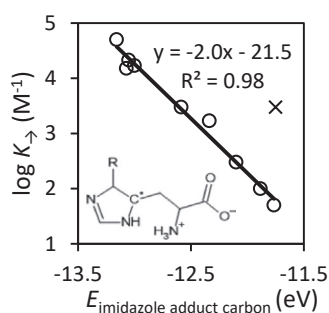
ROS-mediated degradation in play [74,75], Fig. 3. Baseline pO_2 in the luminal intestine is as low as 10^{-6} M [57]; 70–80% of all lymphocytes reside in the GI tract [76], binding ring-contracted products. We find it is not a coincidence that all (neuro/immunological) CMZ side effects involve lower pH/O_2: skin (pH=4.7–5.7), bone marrow (pH=6.7–7.1) [77,78], lymph node pockets (pH~6.3–6.4 [79,80]) and the synaptic gap [81,82] are acidic. Among tissues, bone marrow and skin $[O_2]\leq 2 \times 10^{-5}$ M) can be low in O_2 [80,83].

Aeration during photocatalytic treatment of organic matter produces CO_2 and organic acids depleting O_2 and acidifying water ($CO_2 + H_2O \rightarrow 2H^+ + CO_3^{2-}$) [84–86]. This promotes toxicity (formation of ring-contracted products) by a factor of ~3 [87], matching our result (factor 3, Fig. 3). Indeed, presence of CO_2 promotes forming compounds with higher toxicity [87]. Surface water contains up to 3×10^{-4} M O_2, porewater of 'anaerobic' peatland soil contains as low as ~1 × 10^{-6} M O_2 [88]. The difference profoundly influences the CMZ transformation. Sand/peat soils and grassland meadows are generally more acidic (pH=4.5–5.5); decrease in pO_2 therein would deteriorate toxicity even more (diagonal in Fig. 3). Reducing pH (7.8→7.1), elevated CMZ toxicity to clams (survival; oxidative stress) by a factor 1–2 over single stressors (i.e., low pH or CMZ alone) [89], matching our results (Fig. 3).

3.2. Radical cations – interaction with OH^-

Importance of E_{HOMO} of CMZ-OH$^\bullet$ (Fig. 5A) shows that the forward- and backward reactions are driven by enthalpic product formation. ΔG_{CS} during the transition state (Eq. 2) appears not significant [90]. To obtain k and K for addition/elimination of OH^- by hydroxylated CMZ (CMZ-OH$^\bullet$, $E_{HOMO} = -9.4$ eV) we used the model in Fig. 5A. The SOMO of the doublet cation radical (CMZ$^{\bullet+}$) interacts with the highest occupied molecular orbital (HOMO) of the singlet OH^- to form a new bond: the HOMO of CMZ-OH$^\bullet$. E_{HOMO} and structure of CMZ-OH$^\bullet$ are within model applicability domain (Fig. 5A). Based thereon, we calculate $k_\rightarrow = 10^{8.3}$ M^{-1}s^{-1}, $k_\leftarrow$ $10^{4.5}$ s^{-1} for addition of OH^- to the cation, and elimination of OH^-, respectively.

Under O_2-free (N_2O-saturated) conditions the CMZ-OH$^\bullet$ radical decays to a species with a higher value of λ_{max}, > 375 nm. λ_{max} increases over time (Fig. 4A); we observed a buildup around 425 nm: the wavelength generally attributed to a radical cation [61,90–94]. Radical cation absorptivity is indeed generally lower than that of OH-adducts [91], Fig. 4B. The buildup takes ~10 μs, which agrees (ln(2)/10^{-5} s^{-1}, Fig. 4A,B) with our predicted $k_\leftarrow$. We thus deem k values reliable. According to Eq. 3, the values imply an equilibrium constant K for elimination of OH^- is $10^{4.5}/10^{8.3} = 10^{-3.8}$ M. For simultaneous elimination of OH^- and ring-closure by purines K = $10^{-4.4}$ M was reported [95]: slightly lower, probably due to extra entropic cost. $10^{-3.8}$ M means that equilibrium dictates (Eq. 4, for pH~7.4) $10^{-3.8}$M/$10^{-(14-7.4)}$M = 630 times more CMZ$^{\bullet+}$ than there is CMZ-OH$^\bullet$:

$$K_{OHelim} / [OH^-] = [CMZ^{\bullet+}] / [CMZ-OH^\bullet] = 630 \text{ (at pH~7·4)} \quad (6)$$

3.3. Radical cations – interaction with H_2O

Dependency of radical cation formation on H^+ concentration suggests protonation of the OH-adduct might be a precursor step, followed by elimination of H_2O [90]. Even if H^+-catalyzed (e.g., $10^{-4.4}$ M) H_2O elimination is fast (10^9 s^{-1}), H_2O elimination (CMZ-OH$^\bullet$ + H^+ → CMZ$^+$ + H_2O) does not outweigh OH^- elimination $10^{4.5}$ s^{-1}: multiplying k ~1 × 10^9 M^{-1}s^{-1} [61,90] with $[H^+]$ = $10^{-7.4}$ M gives 40 s^{-1}, implying 40 s^{-1} for H_2O elimination forming CMZ$^+$ (pH7.4) [90], not significantly competing with formation of CMZ$^+$ via OH^- elimination ($10^{4.5}$ s^{-1}). Thus, $k_{elimH2O,OH^-}=k_{elimH2O^\bullet}\cdot[H^+] + k_{elimOH^-}=k_{elimOH^-}$ (pH>4.5) [96]. When pH is ~3 units lower, H_2O elimination may start competing: ~$10^{-4.4} \times 10^9 = 10^{4.6}$ s^{-1} (Fig. 5).

Fig. 2–2. Equilibrium constants (K) for radical (R) addition onto the imidazole group of histidine. x-values are closed-shell orbital energies of imidazole radical adducts localized on β-carbon atoms. y-values are K values for radicals (R). Data from [66].
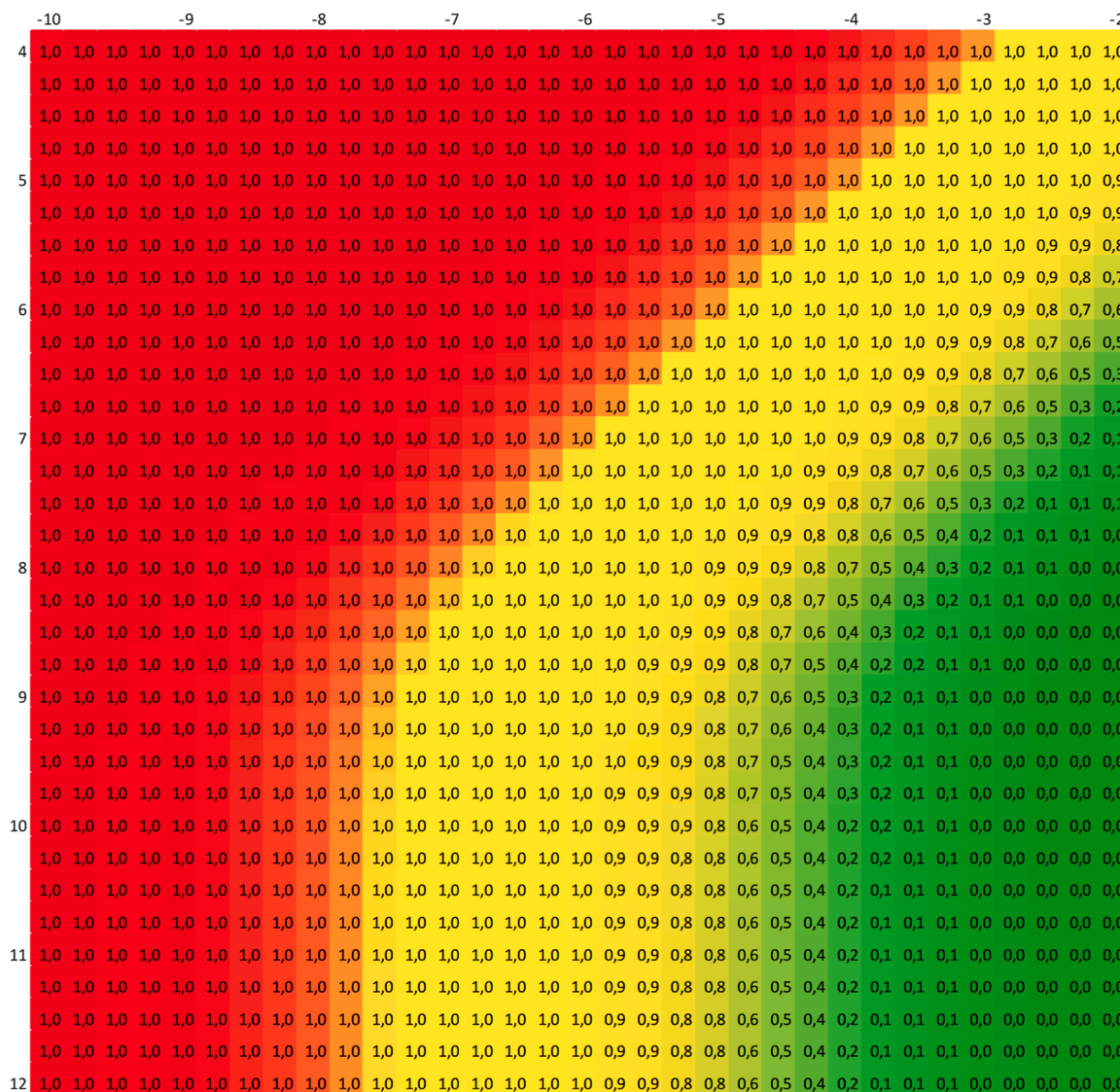
Fig. 3. Heat map plot of toxicity (Eq. 9), given as $K_{tox}/(1 + K_{tox})$. With pH on the vertical y-axis and pO_2 on the horizontal x-axis. Red: increased toxicity, green: reduced toxicity. 'Standard conditions' are pH = 7.4; $pO_2 \sim 3 \times 10^{-4}$ M. With minimal toxic products: $toxicity_{K_{tox} \to 0} = 0$. (Non-)toxic concentrations are equal when K_{tox} is 1: $toxicity_{K_{tox} \to 1} = 0.5$. Effects double (goes to 1) when K_{tox} goes to infinity: $toxicity_{K_{tox} \to \infty} = 1$.
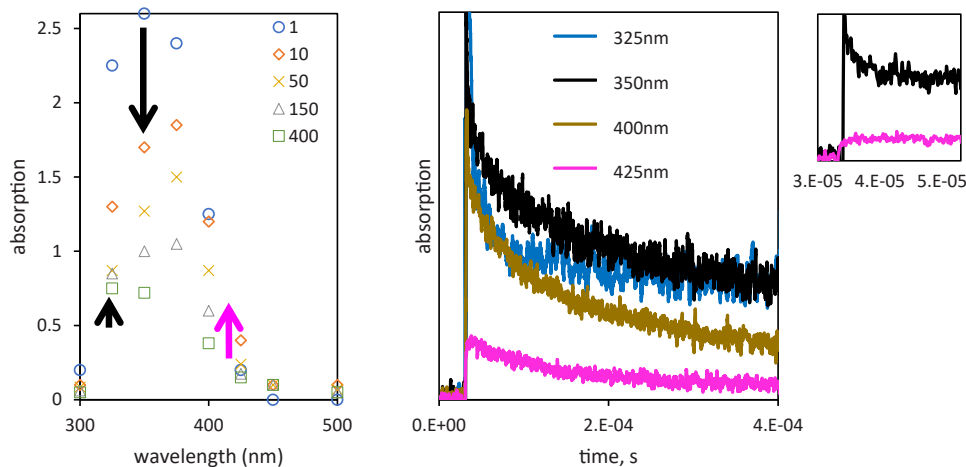

Fig. 4. A. Time resolved (μs) spectrum of irradiated N_2O-saturated CMZ solution. A small peak at 600 nm might be from the solvated electron e_{aq}^-, which appears to disappear after only a few microseconds. In N_2O-saturated solutions. We attribute the equilibration reaction in the first microseconds to water elimination/addition by a CMZ cation. y in photons·cm^{-2} (10^{15}).

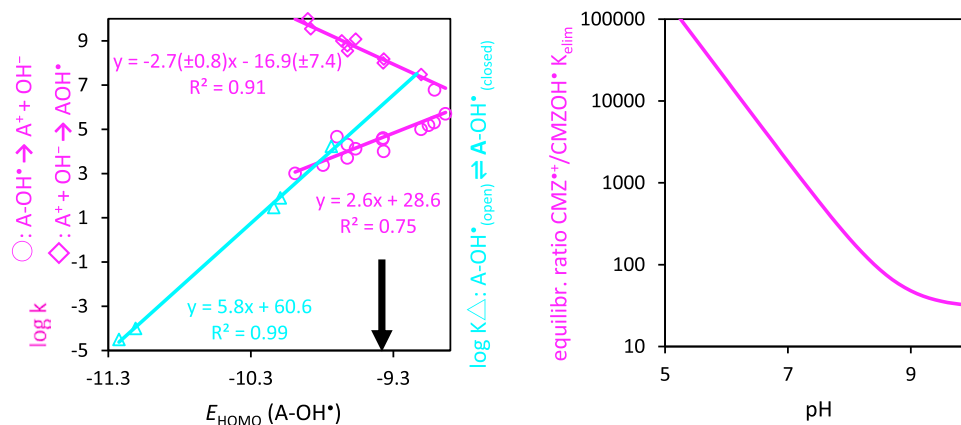**Fig. 5.** A. Regressions between log k, log K and E_{HOMO}. The arrow denotes CMZ-OH$^\bullet$. Data for mono/polycyclic aromatics from [90] and [97]. k represents a mix of OH-adducts, but we took the major species. Blue data [98,99]: K for a terpene-radical (middle triangle) from $e^{-(\Delta H-T\Delta S)/RT}$, with $\Delta H = 27$ kJmol^{-1} [100] and TΔS 19kJmol^{-1} [101–103] for conformational strain weakening intramolecular bonding. B: The position of the equilibrium varying with pH. $K_{elim} = (k_{H2Oelim} + k_{OH-elim})$ / $(k_{H2Oadd} \times [H_2O] + k_{OHadd} \times [OH^-])$, where we take $k_{H2Oelim} = k_{prot} \times [H^+]$ and pH above 4.5, so that $K_{elim} = (k_{OH-elim})$ / $(k_{H2Oadd} \times [H_2O] + k_{OHadd} \times [OH^-])$. $k_{H2Oadd} \times [H_2O]$, $k_{OHadd} \times [OH^-]$ and $k_{prot} \times [H^+]$ are pseudo-1st order k at specific pH [96].

A power law ($k_{H2O} = 3 \times 10^{-16} \times k_{OH-}^{2.02}$ (R^2 = 0.996 [90]) shows that addition of H$_2$O onto the cation is slower 1.9×10^1 M^{-1}s^{-1}. The power law implies that the overall H$_2$O elimination involves 2 H$_2$O molecules: an additional acid/base reaction. The pK$_a$ of CMZ-OH$_2^{\bullet+}$ is $\lesssim 0$ [90,94, 104], as its reduction potential is ~1 eV higher than CMZ-OH$^\bullet$ [105, 106]. Thus, in toxicological and environmental situations, [CMZ-OH$_2^{\bullet+}$] is negligible compared to [CMZ-OH$^\bullet$]. Absorption attributable to OH$_2^+$ adducts are not usually observed, thus half-lives of OH$_2^+$ adducts are short [90]. Elimination of H$_2$O may be stepwise, with first fast deprotonation (H$^+$ elimination); then elimination of OH$^-$ occurring[2] by $k_{OH-elim} = 10^{4.5}$ s^{-1}. Then the equilibrium constant K for elimination of H$_2$O is $10^{4.5}$ / 1.9×10^1 = 1.7×10^3 M. In H$_2$O (55.5 M) under equilibrium it implies: 1.7×10^3 / 55.5 = 30 times more CMZ$^{\bullet+}$ than there is CMZ-OH$_2^{\bullet+}$. This value is lower than 630 (K for elimination by CMZ-OH$^\bullet$); thus 30 is the limiting ratio [CMZ$^{\bullet+}$]/[CMZ-OH$_{(2)}^{\bullet(+)}$] at high (er) pH where OH$^-$ attacks the cation, Fig. 5B.

$$K_{H2Oelim} / [H_2O] = [CMZ^{\bullet+}] / [CMZ-OH_2^{\bullet+}] = 30 (all\ pH) \qquad (7)$$

K values by Moro at a high pH limit show a ratio of 10 (303 M^{-1} $\times10^{-1.5}$ M) [104], corroborating our value of 30, though Moro did specify elimination of OH$^-$. Governed by fast pK$_a$/pH equilibration, the CMZ-OH$_2^{\bullet+}$ concentration increases with acidity via [CMZ-OH$_2^{\bullet+}$] = ([CMZ-OH$^\bullet$] $\times$ [H$^+$]) / 10^{-pKa} but in H$_2$O the ratio [CMZ-OH$_2^{\bullet+}$]/[CMZ$^{\bullet+}$] stays the same.

A ratio of 30 at room temperature means $\Delta G = -2.5 \times \ln(30)$ = -8.5 kJ/mol and favorable and enthalpy-controlled elimination. -8.5 kJ/mol equates to (π) 'bond' energies between H$_2$O and aromatic cations [55,107–109] which, upon elimination, break to release entropy, offsetting enthalpy increase [110]. In addition to orbital energies, we might expect steric factors and charge to affect K (Figs. 5A and 2–2), moreso for structures [111] more complex than CMZ. Underlying data (Figs. 5A and 2–2) did not specify the nature of the carbon-oxygen bond in OH-CMZ adducts, e.g., π- or σ-adduct [112]. In comparison, energies (Figs. 5A and 2–2) are derived based on energy-minimization of structures and evaluation of electron densities. Considering the strength of the regressions, these calculations may be able to evaluate the nature of the bonding in (local) equilibria. Given structural similarity (of CMZ to structures in Fig. 5A) and broad applicability of frontier molecular orbital (FMO) energies (Fig. 2–2) [55,65,108,113,114], we regard predicted K for radical species of CMZ tentatively reliable.

3.4. Ring opening/closing

The CMZ-OH$^\bullet$ adduct (2_{ox}) may fragment into a ring-opened product. In absence of data, we obtain K for opening/closing from Fig. 5A and mechanistic considerations. The regression in Fig. 5A predicts for the cumyloxyl radical ($E_{HOMO}=-10.4$ eV) and succinimidyl radical ($E_{HOMO}=-11.2$ eV) K values of 1 and 10^{-4} resp., comparable with literature K= 0.1 ($k_{closure}\leq 8 \times10^7$; $k_{opening}$=7.5 $\times10^8$ s^{-1} [115]) and experimental $K\approx 10^{-3}$ [116]. Given the agreement, Fig. 5A is tentatively reliable, and predicts for CMZ-OH$^\bullet$ ($E_{HOMO}=-9.4$ eV) K= $10^{6.0}$. The high value indicates a high driving force for closure. As sp^2 radicals are more reactive, closure by sp^2 carbon radicals (like CMZ-OH$^\bullet$) is faster (~10^9 s^{-1}) than for sp^3 carbon radicals (10^4–10^6 s^{-1}), reflected by higher bond dissociation energy of sp^2–sp^3 than sp^3–sp^3 [117]. The radical on CMZ-OH$^\bullet$ is resonance-stabilized by a π (aryl) system, and experiments [118,119] indicate slow CMZ-OH$^\bullet$ ring opening (to 3_{ox}, Fig. 2). Ring strain and electron withdrawing groups can increase cyclization [120,121], more favorable and in water, polar or protic solvents [61,100,116,122–124] (Fig. 5A [98]). Thus, K= $10^{6.0}$ for CMZ-OH$^\bullet$ ring closure/opening is a minimum. As $K_{CMZ-OHopen/closed} << K_{CMZ^{\bullet+}/CMZ-OH_2^+}/55.5$ ($10^{-6} << 30$) we can largely neglect its contribution.

3.5. Reaction with O$_2$

While CMZ-OH$^\bullet$ breaks down anaerobically, we do not expect buildup of CMZ-OH-O$_2^\bullet$ at ~375 nm (maximum absorption in Fig. 4A), as it has $\lambda_{max}\leq 300$ nm. We observe fast decay of the hydroxycyclohexadienyl radical (CMZ-OH$^\bullet$, λ_{max}~350–375 nm) at 375 nm (10^{-6} s). The 375 nm decay does not appear (DT50 $\approx 1\mu$s) distinct from cation formation (1–10μs), matching buildup at 425 nm. We see a stable plateau forming via the fast decay. But, were the decay due to cation formation, the absorption signal should go to 0, as K= 630 at pH7.4. We conclude that the decay cannot be due to cation formation; they are separate reactions. As strictly λ_{max}(CMZ-H$^\bullet$) $\neq \lambda_{max}$(CMZ-OH$^\bullet$) [91] and yield of CMZ-H$^\bullet$ radicals is too low (10%), decay of CMZ-H$^\bullet$ cannot explain the (>)20% (0.5/2.5) decrease in spectral absorption.

The spectrum (~10 µs) indicates that we worked in near O$_2$-free conditions, as presence O$_2$ would (further) reduce absorption at 375 nm, and increase absorption (hydroxycyclohexadienyl-O$_2$ radical ~ 500 M^{-1}cm^{-1} [125]) ~290–300 nm [126,127]. Based on energetics, we expect the k for addition of O$_2$ to CMZ-OH$^\bullet$ to be near the diffusion limit. For CMZ-OH$^\bullet$: $E_{SOMO}= -4.9$ eV and for the CMZ-OH-O$_2^\bullet$-adduct: $E_{SOMO}= -5.4$ eV, $E_{LUMO}= -0.45$ eV. Using formulas 4,5 [65] and these values we calculate $k_r = 1 \times 10^9$ M^{-1}s^{-1}. Even at low O$_2$ concentration

---

[2] the elimination rate is [CMZ-OH$_2^+$] $\times$ $k_{H2Oelim}$ + [CMZ-OH] $\times$ $k_{OH-elim}$, but as [CMZ-OH] $>>$ [CMZ-OH$_2^+$], elimination rate is [CMZ-OH] x $k_{OH-elim}$

(1 μM [128–130]) the expected decay of the CMZ-OH$^\bullet$ is $\sim 1 \times 10^6$ s^{-1}; indeed, we found the decay of 1×10^6 s^{-1} (DT50 ≈ 1 μs), Fig. 6. This affirms the k for CMZ-OH$^\bullet$ + O$_2$ → CMZ-OHO$_2^\bullet$ of $\sim 1 \times 10^9$ M^{-1}s^{-1}. The value agrees with experiments for O$_2$ addition on polycyclics in which the unpaired electron resides on carbon: $10^{8.7-9.0}$ (naphthalene, 8-methylflavone [131,132]), close to the diffusion limit.

3.6. Oxygen-adduct stability

The plateau formation hints to an equilibrium between the CMZ-OH-O$_2^\bullet$ adduct and the CMZ-OH$^\bullet$ + O$_2$ system. The plateau shows that addition is reversible, as Fang et al. also found for benzene analogs [126]. We compared the height of this plateau with the maximum absorption height (2:2.5). We see that $\sim$20% of the CMZ-OH$^\bullet$ radicals may attain a O$_2$ at a concentration of ~ 1 μM. 1 Gy equates to 0.1036 mmol primary radicals per Gy. Thus, irradiating N$_2$O-saturated solutions with ~ 7 Gy (G = 5.35) (Fig. 6) forms 3.8 mmol OH$^\bullet$. For a 1 ml cell this means 3.8 μM, in line with similar radiolysis experiments [97]. When CMZ acts as the sole scavenger of OH$^\bullet$, it means that 20% of $\sim$3.8 μM CMZ-OH$^\bullet$ radicals attain O$_2$: [CMZ-OH-O$_2^\bullet$] = 0.76 μM.

Equilibration reduces the O$_2$ concentration from ~ 1 μM by 0.76 μM to $\sim$0.24 μM, and CMZ-OH$^\bullet$ to $\sim$3.04 μM. K is defined by Eq. 8:

$$K = [\text{CMZ-OH-O}_2^\bullet] / ([\text{CMZ-OH}^\bullet] \times [\text{O}_2]) \tag{8}$$

By which we obtain $K = 0.76 / (3.04 \times 0.24) = \sim 1 \times 10^6$ M^{-1}. This is higher than values recorded by Fang et al. (0.33–2.6 $\times 10^4$ M^{-1}) for benzene-derived radicals, indicating a stabilizing contribution of additional π electrons in CMZ. Substances like O$_2$ prominently interact via π-bonding [133,134] with aromatics and d-block complexes [135]. Hard Lewis acid/base interactions may strengthen the bond, forming a 'stable' CMZ$^{\bullet+}$-O$_2^{\bullet-}$ like system, i.e., (super)oxide anion-cation ionogenic bonding [65,136]. O$_2$ 'traps' (captures) the CMZ-OH$^\bullet$ adduct to limit it eliminating OH$^-$. Boltzmann ($\Delta G = -RT \times \ln K$) gives a value for ΔG of -34 kJ/mol, reflecting polar bonding [109,137]. It also implies 1×10^9 M^{-1}s^{-1}/ 1×10^6 M^{-1} = $\sim 1 \times 10^3$ s^{-1} for the backward reaction, comparable to elimination of O$_2$ by adducts of terephthalate (3.4 $\times 10^3$ s^{-1}) [126] and styrene sulfonate ($\leq 4.5 \times 10^3$ s^{-1}) [127] as well as superoxide elimination ($\sim 10^{2-3}$ s^{-1}) [127,138].

4. Uncertainties

The depth of uncovered side reactions possible affects the accuracy of our approach. The nature of intermediate species (Section 3.3) drives observed behaviors, and validity of assumptions on kinetics (Methods 2.3). Central to neuroimmunological responses is the formation of the
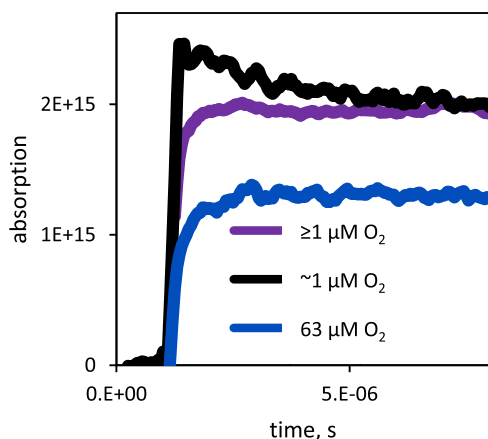

Fig. 6. Absorption (photons cm^{-2} Gy^{-1}) recorded at 375 nm of a solution of carbamazepine (300 μM, pH$\sim$7.4), saturated with N$_2$O gas, irradiated with $\sim$10 Gy. Kinetic traces depict ~ 1 μM O$_2$ (top) and > 1 μM O$_2$ (middle).

aldehyde 3$_{anox}$, Figs. 2, 7B. We presumed competing equilibria to drive the formation of, e.g., 3$_{anox}$: thermodynamic control of product formation. Under various pH/pO$_2$ thermodynamics apparently favors production of radical cations (Fig. 3). Lower CMZ-OH$^\bullet$ concentrations via reaction with O$_2$ reduce cation formation, because elimination of OH$^-$ is slow ($10^{4.5}$ s^{-1}). Toxicity then becomes kinetically controlled. Follow-up reactions (i.e., after the equilibria) may add to kinetic control. Speeds of the respective degradations following the equilibria will affect overall toxicity. In absence of O$_2$, the CMZ-OH$^\bullet$ decays ($10^{4.4\pm1.1}$ s^{-1}), which we ascribe to an additive mix of e.g. ring opening/contraction, OOH$^\bullet$ elimination and H-shift, Fig. 2. Ring contraction towards 3$_{anox}$ is fast due to resonance stabilization (Fig. 2); closure may be observed $\lessapprox 10^3$ s^{-1} ($<10^{-6} \times \sim 10^9$ s^{-1}), comparable to decomposition of the peroxyl via O$_2^{\bullet-}$ elimination (0.3–1.1 $\times 10^3$ s^{-1} [127]). Termination, bimolecular decay, H-shifts and rearrangements occur by 10^{2-3} and $\sim 10^3$ s^{-1} [97, 139,140], Fig. 2.

As pathways in biological systems are often optimized towards each other [141], we have little reason to assume that follow-up reactions have substantially different speeds. We tentatively regard these having minimal effect: only when a specific follow-up reaction substantially outweighs another it may aid fine-tuning our toxicity calculations. Structure 1$_{ox}$ (Fig. 2) might rearrange to form an epoxide, which is a known precursor to mutagenic response [142], but glucuronidation of the alcohol 2$_{ox}$ may detoxify CMZ [143]. Both render aerobic toxicity uncertain. At pH< 4 there may be supplemental cation formation via H$^+$-catalyzed H$_2$O elimination. Presence of O$_2$ during radical generation yields superoxide: H$^\bullet$ + O$_2$ → O$_2^{\bullet-}$ + H$^+$; E$_{aq}^-$ + O$_2$ → O$_2^{\bullet-}$ (2.1 $\times 10^{10}$; 1.9 $\times 10^{10}$ M^{-1}s^{-1}) but reaction with CMZ is too slow to effect kinetic traces: k$_r$(O$_2^{\bullet-}$) = $10^{-2.5 \ ELUMO+3.2} = 10^{5.2\pm1.0}$ M^{-1}s^{-1} [108]. Secondary buildup at 325 nm ($\sim 10^{-4}$ s, Fig. 4) may be e.g., formation of a ring-contracted product, CMZ-OH (CMZ-OH-O$_2^\bullet$ that eliminated HO$_2^\bullet$). Apart from the central CMZ bond, attack elsewhere gives a mix of OH$^\bullet$- (and H$^\bullet$-) adducts. The complexity of competing pathways/species requires future (product) analysis. (Side) reactions e.g., production of O$_2^{\bullet-}$ (broad λ_{max}=241 nm [144]) complicate observing CMZ-OH-O$_2^\bullet$ adducts (<300 nm). Limiting bimolecular decay requires low dosing, which gives low yields and resolution, warranting alternative techniques. An iterative computational-experimental approach aid the way forward.

5. Outlook

Toxicities of transformation products (aldehyde, imine, carboxylate in Fig. 1) vary by a factor $\sim$300 (Table 1) due to AChR inhibition (blocking). The value of K_{tox} in Eq. 2 characterizes relative concentrations, not pharma/toxicological activity. Considering negligible toxicity of 3$_{ox}$, we can 'adjust' K_{tox} by considering toxicity as a function of fractional binding of receptors [145]:

$$toxicity \quad induction \quad potential \propto \frac{K_{tox}}{K_d + K_{tox}} \tag{9}$$

With K_d as an equilibrium dissociation/binding constant. When disregarding (receptor) binding, $K_d = 0$. We can attribute differences in toxicity (Table 1) to binding, K_d in Eq. 9. Anionic residues form a (cation) binding site in AChR [146], bound also by tyrosyl via cation-π interaction [147,148], positioning the acetylcholine ester optimally in the active site [149] to allow hydrolysis [150]. Low (neuro)immunological pH (e.g., <6 at the synaptic site) produces an (iminium) cation (pK$_a$$\gtrsim$6 [151,152]) binding the AChR 10–100 times (6–11 kJ/mol) stronger (lower K_d in Eq. 9), Fig. 7A. Proton exchange and resonance stabilize and distribute the cationic (imidinium) charge throughout the molecule (Fig. 7B), facilitating cation-π interaction with the AChR tyrosyl [148,153]. The iminium reacts with tyrosyl under mild acidity [150,154], e.g. cyclizing into an non-planar 8-membered indolo-azocine ring (Fig. 7B), with a shapes and structures among those of the most powerful AChR-binding toxins in the world [155,156], inhibiting hydrolysis of neurotransmitters. Like cationic indoles also drive
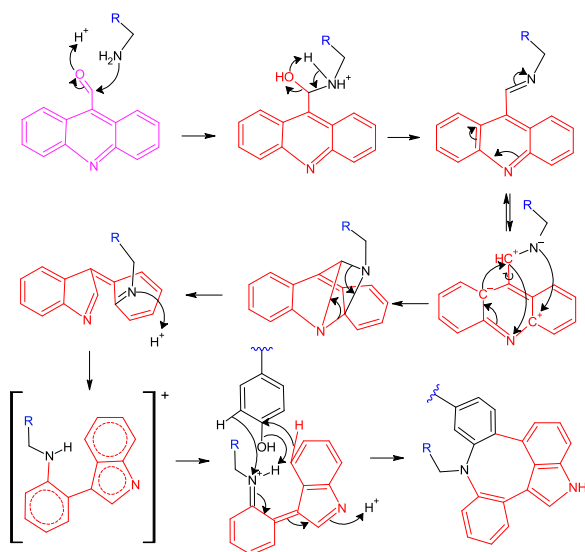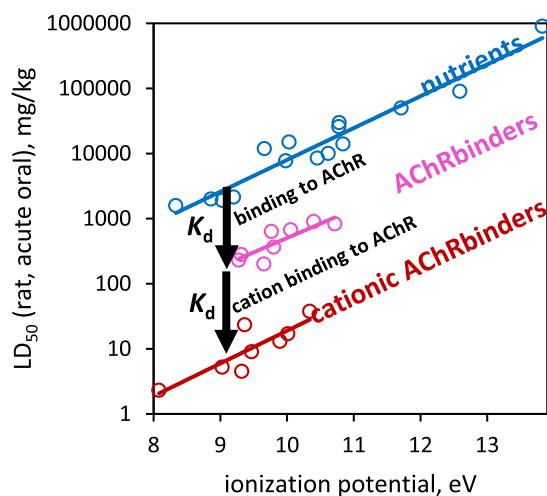
Fig. 7. A. Lethal dose 50 versus ionization potential of vitamins, sugars, etc. (blue), neutrally-charged AChR-binders (e.g., herbicides, magenta), and cationic AChR-binders (LD_{50} data from [161–163]). Downward arrows denote toxicity change that carbamazepine undergoes upon radical-mediated transformation. 7B: hypothesized pathway for iminium-modification of acridine carboxyaldehyde and binding to tyrosine in the anionic AChR binding pocket: along the pathway, K_d decreases.

immunological response [157,158] by targeting (mitochondial) AChR [159,160].

Predicting transformation products and toxicity facilitates risk assessment for 100,000 + substances. In this bigger picture, we presented a case study for carbamazepine (CMZ), a pharmaceutical with ecotoxic and neuro-immunologic side effects. We evaluated toxicity via mechanism- and redox-based calculus elucidating complex modes of action, covering multiple speciation states and conditions [59,164]. Despite aforementioned uncertainties, results are in agreement with toxicity assays, demonstrating that our 'generic' thermodynamic model serves as a bridge between chemistry and (eco)toxicology. We expect the equilibrium-based approach useful to evaluate substances and conditions 'similar' to the current case study by interpolation (Figs. 5 and 7). The present case study on CMZ paves the way for toxicity calculus in terms of thermokinetics and speciation for other substances. Future efforts should test a broader range of substances and conditions like aromatic AChR binders (Fig. 7) to move from single substances to classes of substances. Having substantiated the domain of applicability, we anticipate implementation in a range of applications, e.g., for lab-field

extrapolation [165], tackling mixture assessments [166,167], food-drug interaction [168] and elucidation of immunological and enzymatic variation [23]. In addition, our approach may facilitate fine-tuning of drug dosing or detoxification [5,169] to mediate interplay between medicinal and toxicological properties.

Declaration of Competing Interest

The authors declare that they have no known competing financial interests or personal relationships that could have appeared to influence the work reported in this paper.

Data availability

Data will be made available on request.

Acknowledgements

References

[1] European Chemicals Agency, Annual Report 2019. ECHA-20-R-04-EN. ISBN: 978–92-9481–399-2. 2020.

[2] A.J. Hendriks, How to deal with 100,000+substances, sites, and species: overarching principles in environmental risk assessment, Environ. Sci. Technol. 47 (8) (2013) 3546–3547.

[3] J.L. Reymond, The chemical space project, Acc. Chem. Res. 48 (3) (2015) 722–730.

[4] Y. Kawata, et al., Pharmacological discrimination between effects of carbamazepine on hippocampal basal, Ca2+- and K+-evoked serotonin release, Br. J. Pharmacol. 133 (4) (2001) 557–567.

[5] D. Fluyau, N. Revadigar, B.E. Manobianco, Challenges of the pharmacological management of benzodiazepine withdrawal, dependence, and discontinuation, Ther. Adv. Psychopharmacol. 8 (5) (2018) 147–168.

[6] J.L. Wilkinson, et al., Pharmaceutical pollution of the world's rivers, Proc. Natl. Acad. Sci (8) (2022) 119.

[7] H. Breton, D. Hillaire-Buys, Evaluation of carbamazepine reactive metabolites in epileptic patients, Epilepsies 17 (2) (2005).

[8] S.R. Jahromi, et al., Gastrointestinal adverse effects of antiepileptic drugs in intractable epileptic patients, Seizure-Eur. J. Epilepsy 20 (4) (2011) 343–346.

[9] M. Leclercq, et al., Presence and fate of carbamazepine, oxcarbazepine, and seven of their metabolites at wastewater treatment plants, Arch. Environ. Contam. Toxicol. 56 (3) (2009) 408–415.

[10] F.I. Hai, et al., Carbamazepine as a possible anthropogenic marker in water: occurrences, toxicological effects, regulations and removal by wastewater treatment technologies, Water 10 (2) (2018).

[11] D.D. Barcellos, et al., Priority pharmaceutical micropollutants and feasible management initiatives to control water pollution from the perspective of stakeholders in metropolis of Southern Brazil, Integr. Environ. Assess. Manag. 16 (6) (2020) 955–967.

[12] N. Liu, et al., Occurrence and multiple-level ecological risk assessment of pharmaceuticals and personal care products (PPCPs) in two shallow lakes of China, Environ. Sci. Eur. 32 (1) (2020).

[13] N. De la Cruz, et al., Degradation of emergent contaminants by UV, UV/H2O2 and neutral photo-Fenton at pilot scale in a domestic wastewater treatment plant, Water Res. 47 (15) (2013) 5836–5845.

[14] E. Donner, et al., Ecotoxicity of carbamazepine and its UV photolysis transformation products, Sci. Total Environ. 443 (2013) 870–876.

[15] S.M. Furst, et al., Covalent binding of carbamazepine oxidative metabolites to neutrophils, Drug Metab. Dispos. 23 (5) (1995) 590–594.

[16] S.M. Furst, J.P. Uetrecht, The effect of carbamazepine and its reactive metabolite, 9-acridine carboxaldehyde, on immune cell-function in-vitro, Int. J. Immunopharmacol. 17 (5) (1995) 445–452.

[17] Y.L. Zhao, et al., Acute and chronic toxicity of indole alkaloids from leaves of alstonia scholaris (L.) R. Br. in Mice and Rats, Nat. Prod. Bioprospecting 10 (2) (2020) 77–88.

[18] J.E. Saxton, et al., Indole alkaliods. Bisindole alkaloids, ISBN 0-85186-257-8, S. JE, Editor. The Alkaloids: v. 1: A Review of Chemical Literature. Specialist Periodical Reports, Royal Society of Chemistry, Cambridge, Eng, 1971, pp. 150–338.

[19] M. Welliver, Consideration of acetylcholine antagonists for nausea and vomiting, Gastroenterol. Nurs. 38 (4) (2015) 319–321.

[20] S. Sommerlatte, et al., The activation of muscarinic acetylcholine receptors influences the ontogeny of neutrophils. Poster Presentation, SAT0011, Innate Immun. Rheum. Dis. 76 (2017) 772.

[21] L. Zhang, et al., N-acetylcholine receptors regulate cytokines expression and neutrophils recruitment via MAPK/ERK signaling in zebrafish, Dev. Comp. Immunol. 128 (2022).

[22] J.C. Jaen, et al., Acetylcholinesterase inhibition by fused dihydroquinazoline compounds, Bioorg. Med. Chem. Lett. 6 (6) (1996) 737–742.

[23] Mayo Clinic Laboratories, Carbamazepine hypersensitivity pharmacogenomics, varies, Test. Id: CARBR (2022). ⟨https://www.mayocliniclabs.com/test-catalog/overview/610048⟩.

[24] Y. Wu, et al., Activation of T cells by carbamazepine and carbamazepine metabolites, J. Allergy Clin. Immunol. 118 (1) (2006) 233–241.

[25] M. Gunaldi, et al., Carbamazepine and multiple myeloma: possible interaction, Turk. J. Hematol. 30 (1) (2013) 83–84.

[26] J.R. Hughes, M. DeTolve-Donoghue, Chronic leukopenia associated with carbamazepine and other antiepileptic drugs, J. Epilepsy 8 (4) (1995) 282–288.

[27] J. Simko, J. Horacek, Carbamazepine and risk of hypothyroidism: a prospective study, Acta Neurol. Scand. 116 (5) (2007) 317–321.

[28] USEPA Estimation Programs Interface SuiteTM for Microsoft® Windows, v 4.1.1 2012 Washington, DC, USA.

[29] ICCVAM-sponsored validation study (2006) on the use of in vitro basal cytotoxicity test methods to determine starting doses for in vivo acute oral toxicity test. Submissions to U.S. EPA of six-pack acute toxicity studies for pesticide registration. Data provided for the Predictive Models for Acute Oral Systemic Toxicity collaborative modeling effort.

[30] National Library of Medicine (NLM). 2022.ChemIDplus - a TOXNET database. NationalInstitutes of Health, U.S. Library of Medicine. https://chem.nlm.nih.gov/chemidplus/.

[31] Haz-Map, Information on Hazardous Chemicals and Occupational Diseases. Record Name: Proflavine hemisulfate. ⟨https://haz-map.com/⟩. 2022. Olympia, WA, United States, 98501.

[32] J. Gieldanowski, et al., Preclinical pharmacologic investigations on a new group of acridine derivatives with oncostatic activity. I. Acute and subchronic action, Arch. Immunol. Ther. Exp. 28 (5) (1980) 735–754.

[33] the compounds: 3,4-dihydro-3-((4-bromo-2-fluorophenyl)methyl)-2,4-dioxo-7-fluoro-1(2H)-Quinazolineacetic acid, Zenarestat, and the ethyl ester of 5-(3,4-dihydro-2-ethyl-4-oxoquinazolin-3-yl)-1-methyl-pyrazole-4-carboxylic acid.

[34] A. Bahlmann, et al., Carbamazepine and its metabolites in wastewater: analytical pitfalls and occurrence in Germany and Portugal, Water Res. 57 (2014) 104–114.

[35] Y.N. Han, et al., Insight into the generation of toxic products during chloramination of carbamazepine: kinetics, transformation pathway and toxicity, Sci. Total Environ. 679 (2019) 221–228.

[36] F. Desbiolles, et al., Advances and limits of two model species for ecotoxicological assessment of carbamazepine, two by-products and their mixture at environmental level in freshwater, Water Res. 169 (2020).

[37] J. Singh, et al., Mutagenicity of nitrated polycyclic aromatic hydrocarbons: a QSAR investigation, Chem. Biol. Drug Des. 71 (3) (2008) 230–243.

[38] F.A.D. Ribeiro, M.M.C. Ferreira, QSAR model of the phototoxicity of polycyclic aromatic hydrocarbons, J. Mol. Struct. -Theochem 719 (1–3) (2005) 191–200.

[39] J. Forrest, et al., A comprehensive model for chemical bioavailability and toxicity of organic chemicals based on first principles, Front. Mar. Sci. 1 (2014).

[40] J. Meng, et al., Precision redox: the key for antioxidant pharmacology, Antioxid. Redox Signal 34 (14) (2021) 1069–1082.

[41] C.S. Muller, et al., Concurrent cooperativity and substrate inhibition in the epoxidation of carbamazepine by cytochrome P450 3A4 active site mutants inspired by molecular dynamics simulations, Biochemistry 54 (3) (2015) 711–721.

[42] T. Takayasu, et al., Distribution of carbamazepine and its metabolites carbamazepine-10,11-epoxide and iminostilbene in body fluids and organ tissues in five autopsy cases, Forensic Toxicol. 28 (2) (2010) 124–128.

[43] R.M. Jones, J.W. Mercante, A.S. Neish, Reactive oxygen production induced by the gut microbiota: pharmacotherapeutic implications, Curr. Med. Chem. 19 (10) (2012) 1519–1529.

[44] J. Kauppi, et al., Increased oxidative stress in the proximal stomach of patients with Barrett's Esophagus and adenocarcinoma of the esophagus and esophagogastric junction, Transl. Oncol. 9 (4) (2016) 336–339.

[45] L.P. Candeias, et al., Free hydroxyl radicals are formed on reaction between the neutrophil-derived species superoxide anion and hypochlorous acid, Febs Lett. 333 (1–2) (1993) 151–153.

[46] L.P. Candeias, M.R.L. Stratford, P. Wardman, Formation of Hydroxyl Radicals on Reaction of Hypochlorous Acid with Ferrocyanide, a Model Iron(II) Complex, Free Radic. Res. 20 (4) (1994) 241–249.

[47] Biswas, K., K. Alexander, and M.M. Francis, Reactive Oxygen Species: Angels and Demons in the Life of a Neuron NeuroSci, 2022. 3(1): p. 130–145.

[48] O.A.T. Afuwape, et al., Synaptic vesicle pool-specific modification of neurotransmitter release by intravesicular free radical generation, J. Physiol. Lond. 595 (4) (2017) 1223–1238.

[49] C.C. Chiueh, et al., Intracranial microdialysis of salicylic-acid to detect hydroxyl radical generation through dopamine autooxidation in the caudate-nucleus - effects of MPP+, Free Radic. Biol. Med. 13 (5) (1992) 581–583.

[50] K.Y. Chung, et al., Generation of free radical by interaction of iron with thiols in human plasma and its possible significance, Thromb. Res. 116 (2) (2005) 157–164.

[51] J.K. Im, et al., Carbamazepine degradation by photolysis and titanium dioxide photocatalysis, Water Environ. Res. 84 (7) (2012) 554–561.

[52] T. Tandaric, V. Vrcek, D. Sakic, A quantum chemical study of HOCl-induced transformations of carbamazepine, Org. Biomol. Chem. 14 (46) (2016) 10866–10874.

[53] J. Blotevogel, et al., Quantum chemical prediction of redox reactivity and degradation pathways for aqueous phase contaminants: an example with HMPA, Environ. Sci. Technol. 44 (15) (2010) 5868–5874.

[54] L.P. Hammett, The effect of structure upon the reactions of organic compounds benzene derivatives, J. Am. Chem. Soc. 59 (1937) 96–103.

[55] T.M. Nolte, T. Nauser, L. Gubler, W.J.G.M. Peijnenburg, Thermochemical unification of molecular descriptors to predict radical hydrogen abstraction with low computational cost, PCCP 22 (40) (2020) 23215–23225.

[56] A.M. Ali, et al., Organic contaminants of emerging concern in Norwegian digestates from biogas production (vol 21, pg 1498, 2019), Environ. Sci. Process. Impacts 22 (4) (2020) 1095–1097.

[57] L. Albenberg, et al., Correlation between intraluminal oxygen gradient and radial partitioning of intestinal microbiota, Gastroenterology 147 (5) (2014) 1055.

[58] A. Yazdanbakhsh, et al., Solar photodegradation of carbamazepine from aqueous solutions using a compound parabolic concentrator equipped with a sun tracking system, Open Chem. 17 (1) (2019) 477–484.

[59] T.M. Nolte, et al., Bioconcentration of organotin cations during molting inhibits heterocypris incongruens growth, Environ. Sci. Technol. 54 (22) (2020) 14288–14301.

[60] V. Maeder, et al., Toxic ratio as an indicator of the intrinsic toxicity in the assessment of persistent, bioaccumulative, and toxic chemicals, Environ. Sci. Technol. 38 (13) (2004) 3659–3666.

[61] G.N.R. Tripathi, Electron-transfer component in hydroxyl radical reactions observed by time resolved resonance raman spectroscopy, J. Am. Chem. Soc. 120 (1998) 4161–4166.

[62] X. Zhang, et al., Kinetics and mechanisms of the carbamazepine degradation in aqueous media using novel iodate-assisted photochemical and photocatalytic systems, Sci. Total Environ. 825 (2022), 153817.

[63] L.J. Bu, et al., Insight into carbamazepine degradation by UV/monochloramine: reaction mechanism, oxidation products, and DBPs formation, Water Res. 146 (2018) 288–297.

[64] R.Y. Xiao, et al., Experimental and theoretical insight into hydroxyl and sulfate radicals-mediated degradation of carbamazepine, Environ. Pollut. 257 (2020).

[65] T.M. Nolte, et al., A universal free energy relationship for both hard and soft radical addition in water, J. Phyical Org. Chem. 35 (4) (2021), e4317.

[66] N. Santschi, T. Nauser, An experimental radical electrophilicity index, Chemphyschem 18 (21) (2017) 2973–2976.

[67] T. Nauser, et al., Reversible intramolecular hydrogen transfer between cysteine thiyl radicals and glycine and alanine in model peptides: absolute rate constants derived from pulse radiolysis and laser flash photolysis, J. Phys. Chem. B 112 (47) (2008) 15034–15044.

[68] R.H. Schuler, L.K. Patterson, E. Janata, Yield for the Scavenging of OH Radicals in the Radiolysis of N2O-Saturated Aqueous-Solutions, J. Phys. Chem. 84 (16) (1980) 2088–2089.

[69] C. von Sonntag, The Chemical Basis of Radiation Biology, Taylor & Francis, London, 1987.

[70] R.H. Schuler, A.L. Hartzell, B. Behar, Track effects in radiation-chemistry - concentration-dependence for the Scavenging of OH by Ferrocyanide in N2O-Saturated Aqueous-Solutions, J. Phys. Chem. 85 (2) (1981) 192–199.

[71] J.T. Coin, J.S. Olson, The rate of oxygen uptake by human red blood cells, J. Biol. Chem. 254 (4) (1979) 1178–1190.

[72] M. Falla, G. Giardini, C. Angelini, Recommendations for traveling to altitude with neurological disorders, J. Cent. Nerv. Syst. Dis. 13 (2021), p. 11795735211053448.

[73] I.T. Demchenko, et al., Antiepileptic drugs prevent seizures in hyperbaric oxygen: a novel model of epileptiform activity, Brain Res. 1657 (2017) 347–354.

[74] O. Handa, Y. Naito, T. Yoshikawa, Redox biology and gastric carcinogenesis: the role of Helicobacter pylori, Redox Rep. 16 (1) (2011) 1–7.

[75] D. Bandyopadhyay, A. Chattopadhyay, Reactive oxygen species-induced gastric ulceration: protection by melatonin, Curr. Med. Chem. 13 (10) (2006) 1187–1202.

[76] P. Brandtzaeg, et al., Immunobiology and immunopathology of human gut mucosa - humoral immunity and intraepithelial lymphocytes, Gastroenterology 97 (6) (1989) 1562–1584.

[77] L. Nikolaeva, Features of acid–base balance of bone marrow, Acta Med. Int. 5 (2) (2018) 55.

[78] S.C.A. Yeh, et al., Quantification of bone marrow interstitial pH and calcium concentration by intravital ratiometric imaging, Nat. Commun. 13 (1) (2022).

[79] H. Wu, et al., T-cells produce acidic niches in lymph nodes to suppress their own effector functions, Nat. Commun. 11 (1) (2020).

[80] L.A. Zenewicz, Oxygen Levels and immunological Studies, Front. Immunol. 8 (2017).

[81] A. Sinning, C.A. Hubner, Minireview: pH and synaptic transmission, FEBS Lett. 587 (13) (2013) 1923–1928.

[82] R. Ahdut-Hacohen, et al., Hydrogen ions control synaptic vesicle ion channel activity in Torpedo electromotor neurones, J. Physiol. 556 (Pt 2) (2004) 347–352.

[83] E. Mata-Greenwood, D. Goyal, R. Goyal, Comparative and experimental studies on the genes altered by chronic hypoxia in human brain microendothelial cells, Front. Physiol. 8 (2017).

[84] C.A. Sergides, et al., The structure of hexane soot.3. Ozonation studies, Appl. Spectrosc. 41 (3) (1987) 482–492.

[85] A.V. Levanov, O.Y. Isaikina, A.N. Kharlanov, Kinetics of carbon dioxide release during the ozonation of aqueous solutions of formic acid, Russ. J. Phys. Chem. A 94 (2020) 2219–2225.

[86] M. Larsson, Effects of ozonation/filtration on the raw water from Lake Mälaren. UPTEC W 04 032 Examensarbete. ISSN 1401–5765 M.Sc. Thesis (2004).

[87] E. Kudlek, THe influence of oxygen on the efficiency and the mechanism of carbamazepine decomposition by means of photocatalytic process, Archit. Civ. Eng. Environ. 4 (2015) 93.

[88] J. Hoyos-Santillan, et al., Root oxygen loss from Raphia taedigera palms mediates greenhouse gas emissions in lowland neotropical peatlands, Plant Soil 404 (1–2) (2016) 47–60.

[89] R. Freitas, et al., The impacts of pharmaceutical drugs under ocean acidification: New data on single and combined long-term effects of carbamazepine on Scrobicularia plana, Sci. Total Environ. 541 (2016) 977–985.

[90] J. Holcman, Formation and reactions of radical cations of substituted benzenes in aqueous media. A pulse radiolysis study, Risø National Laboratory, Risø-M (1977) 1947. No.

[91] R. Homlok, et al., Comparison of hydrogen atom and hydroxyl radical reactions with simple aromatic molecules in aqueous solution, Chem. Phys. 534 (2020).

[92] H.S. Fang, et al., Advanced oxidation kinetics and mechanism of preservative propylparaben degradation in aqueous suspension of TiO2 and risk assessment of its degradation products, Environ. Sci. Technol. 47 (6) (2013) 2704–2712.

[93] T. Shida, Y. Nosaka, T. Kato, Electronic absorption-spectra of some cation radicals as compared with ultraviolet photoelectron-spectra, J. Phys. Chem. 82 (6) (1978) 695–698.

[94] S. Dad, et al., Identification and reactivity of the triplet excited state of 5-hydroxytryptophan, J. Photochem. Photobiol. B-Biol. 78 (3) (2005) 245–251.

[95] J.N. Riggins, et al., Kinetic and thermodynamic analysis of the hydrolytic ring-opening of the malondialdehyde-deoxyguanosine adduct, 3-(2'-deoxy-beta-D-erythro-pentofuranosyl)pyrimido[1,2-alpha]purin-10(3H)-one, J. Am. Chem. Soc. 126 (26) (2004) 8237–8243.

[96] T. de Wild, et al., Possible repair mechanism for hydrocarbon-based ionomers following damage by radical attack, J. Electrochem. Soc. 168 (2021), 054514.

[97] N. Zevos, K. Sehested, Pulse-radiolysis of aqueous naphthalene solutions, J. Phys. Chem. 82 (2) (1978) 138–141.

[98] T.A. Halgren, et al., Kinetics and equilibrium constants for reactions of α-Phenyl-Substituted Cyclopropylcarbinyl radicals, J. Am. Chem. Soc. 122 (13) (2000) 2988–2994.

[99] S. Park, T.R. Varick, M. Newcomb, Acceleration of the 4-exo radical cyclization to a synthetically useful rate. Cyclization of the 2,2-dimethyl-5-cyano-4-pentenyl radical, Tetrahedron Lett. 31 (21) (1990) 2975–2978.

[100] J. Světlík, et al., Cerium(IV) based oxidative free radical cyclization of active methylene compounds with some cyclic alkenes: a useful annulation method for terpene functionalization, Tetrahedron 75 (18) (2019) 2652–2663.

[101] C.D. Jones, et al., Lilypad aggregation: localised self-assembly and metal sequestration at a liquid-vapour interface, Chem. Sci. 11 (28) (2020) 7501–7510.

[102] H.P.G. Thompson, G.M. Day, Which conformations make stable crystal structures? Mapping crystalline molecular geometries to the conformational energy landscape, Chem. Sci. 5 (8) (2014) 3173–3182.

[103] NCERT, Chemistry Part II' — NCERT Class 11 Chemistry. Hydrocarbons. 13.2.4 conformations, ISBN 81-7450-535-0, Natl. Counc. Educ. Res. Train. (2022).

[104] A.J. Moro, et al., Chemistry and photochemistry of 2,6-Bis(2-hydroxybenzilidene) cyclohexanone. An example of a compound following the anthocyanins network of chemical reactions, J. Phys. Chem. A 118 (32) (2014) 6208–6215.

[105] A.M.D. Nicholas, D.R. Arnold, Thermochemical parameters for organic radicals and radical ions.1. The estimation of the Pka of radical cations based on thermochemical calculations, Can. J. Chem. Rev. Can. De. Chim. 60 (17) (1982) 2165–2179.

[106] J.J.P. Stewart, MOPAC, Stewart Computational Chemistry, Colorado Springs, CO, USA, 2016.

[107] D. van der Spoel, et al., Thermodynamics of hydrogen bonding in hydrophilic and hydrophobic media, J. Phys. Chem. B 110 (9) (2006) 4393–4398.

[108] T.M. Nolte, W.J.G.M. Peijnenburg, Peijnenburg, Use of quantum-chemical descriptors to analyse reaction rate constants between organic chemicals and superoxide/hydroperoxyl (O-2(center dot-)/HO2 center dot), Free Radic. Res. 52 (10) (2018) 1118–1131.

[109] S. Scheiner, T. Kar, J. Pattanayak, Comparison of various types of hydrogen bonds involving aromatic amino acids, J. Am. Chem. Soc. 124 (44) (2002) 13257–13264.

[110] L. Liu, C. Yang, Q.X. Guo, A study on the enthalpy-entropy compensation in protein unfolding, Biophys. Chem. 84 (3) (2000) 239–251.

[111] J.M. Gebicki, T. Nauser, Fast antioxidant reaction of polyphenols and their metabolites, Antioxidants 10 (8) (2021).

[112] L. Ashton, G.V. Buxton, C.R. Stuart, Temperature-dependence of the rate of reaction of OH with some aromatic-compounds in aqueous-solution - evidence for the formation of a π-complex intermediate, J. Chem. Soc. Faraday Trans. 91 (11) (1995) 1631–1633.

[113] T.M. Nolte, W.J.G.M. Peijnenburg, Aqueous-phase photooxygenation of enes, amines, sulfides and polycyclic aromatics by singlet (a1Δg) oxygen: prediction of rate constants using orbital energies, substituent factors and quantitative structure–property relationships, Environ. Chem. 14 (7) (2018) 442–450.

[114] T.M. Nolte, et al., Transition-state rate theory sheds light on 'black-box' biodegradation algorithms, Green. Chem. (2020).

[115] M. Salamone, et al., Phenyl bridging in ring-substituted cumyloxyl radicals. A product and time-resolved kinetic study, Org. Lett. 11 (11) (2009) 2453–2456.

[116] G. Merenyi, J. Lind, L. Eberson, The return of the succinimidyl radical, Acta Chem. Scand. 52 (1998) 62–66.

[117] H. Togo, Advanced Free Radical Reactions for Organic Synthesis, Elsevier, 2004.

[118] C. Chatgilialoglu, et al., 5-Endo-trig radical cyclizations: disfavored or favored processes, J. Am. Chem. Soc. 124 (36) (2002) 10765–10772.

[119] K.K. Milnes, S.E. Gottschling, K.M. Baines, Determination of the rate constant for ring opening of an alpha-cyclopropylvinyl radical, Org. Biomol. Chem. 2 (23) (2004) 3530–3534.

[120] T.A. Hamlin, et al., Structural distortion of cycloalkynes influences cycloaddition rates both by strain and interaction energies, Chemistry 25 (25) (2019) 6342–6348.

[121] J.M. Baker, W.R. Dolbier, Jr, Density functional theory calculations of the effect of fluorine substitution on the cyclobutylcarbinyl to 4-pentenyl radical rearrangement, J. Org. Chem. 66 (8) (2001) 2662–2666.

[122] V.W. Bowry, J. Lusztyk, K.U. Ingold, Calibration of a New Horologery of Fast Radical "Clocks". Ring-Opening Rates for Ring- and a-Alkyl-Substituted Cyclopropylcarbinyl Radicals and for the Bicycle[2.1.0]pent-2-y1 Radical, J. Am. Chem. Soc. 113 (1991) 5687–5698.

[123] R.W. Taft, et al., Linear solvation energy relations, J. Solut. Chem. 14 (3) (1985) 153–186.

[124] M.J. Kamlet, et al., Linear solvation energy relationships.23. A comprehensive collection of the solvatochromic parameters and some methods for simplifying the generalized solvatochromic equation, J. Org. Chem. 48 (17) (1983) 2877–2887.

[125] X. Pan, C. von Sonntag, OH-Radical-induced oxidation of benzene in the presence of oxygen: R·+O2 ↔ RO2 equilibria in aqueous solution. A pulse radiolysis study, Z. Nat. 45b (1990) 1337–1340.

[126] X.W. Fang, et al., Reversibility in the reaction of cyclohexadienyl radicals with oxygen in aqueous-solution, Chem. A Eur. J. 1 (7) (1995) 423–429.

[127] S.M. Dockheer, et al., Damage to fuel cell membranes. Reaction of HO· with an oligomer of poly(sodium styrene sulfonate) and subsequent reaction with O2, Phys. Chem. Chem. Phys. 12 (45) (2010) 15140. -15140.

[128] Hamilton Gastight SampleLock syringes. Specification Sheet (Part # 81656). 10 ml, Model 1010 SL SYR, Large Removable NDL 22.https://www.hamiltoncompany.com/laboratory-products/syringes/81656.

[129] Hamilton Syringes. 4·Syringes. Konik-Tech. www.konik-group.com. The standard needle dead volume is 6.81 μM, the syringe volume was 10 ml.

[130] Personal communication with Thomas Nauser. With proper use of this syringe one can go down to low O2 concentrations in the order of only 1 μM O2.

[131] M. Roder, L. Wojnarovits, G. Foldiak, Pulse-radiolysis of aqueous-solutions of aromatic-hydrocarbons in the presence of oxygen, Radiat. Phys. Chem. 36 (2) (1990) 175–176.

[132] L.P. Candeias, S.A. Everett, P. Wardman, Free-radical intermediates in the oxidation of flavone-8-acetic acid - possible involvement in its antitumor-activity, Free Radic. Biol. Med. 15 (4) (1993) 385–394.

[133] B.W. Brinkmann, et al., Predicted adsorption affinity for enteric microbial metabolites to metal and carbon nanomaterials, J. Chem. Inf. Model. (2022).

[134] T.M. Nolte, A.M.J. Ragas, A review of quantitative structure-property relationships for the fate of ionizable organic chemicals in water matrices and identification of knowledge gaps, Environ. Sci. Process. Impacts 19 (3) (2017) 221–246.

[135] A.F. Jalbout, L. Adamowicz, Anion-aromatic molecule complex. Ab initio study of the benzene·O2 anion, J. Chem. Phys. 116 (22) (2002) 9672–9676.

[136] C.J. Cramer, et al., Variable character of O-O and M-O bonding in side-on (η2) 1: 1 metal complexes of O2, Proc. Natl. Acad. Sci. 100 (7) (2003) 3635–3640.

[137] Y. Ibrahim, et al., Hydrogen bonding interactions of Pyridine(·+) with water: stepwise solvation of distonic cations, J. Phys. Chem. A 111 (6) (2007) 1006–1014.

[138] P. Neta, R.E. Huie, A.B. Ross, Rate constants for reactions of peroxyl radicals in fluid solutions, J. Phys. Chem. Ref. Data 19 (2) (1990) 413–513.

[139] G.N.R. Tripathi, Electron-transfer component in hydroxyl radical reactions observed by time resolved resonance Raman spectroscopy, J. Am. Chem. Soc. 120 (17) (1998) 4161–4166.

[140] M.L. Grimm, et al., Stereoelectronic and resonance effects on the rate of ring opening of N-cyclopropyl-based single electron transfer probes, J. Am. Chem. Soc. 142 (5) (2020) 2640–2652.

[141] T.M. Nolte, et al., Transition-state rate theory sheds light on 'black-box' biodegradation algorithms, Green. Chem. 22 (11) (2020) 3558–3571.

[142] A.W. Wood, et al., Mutagenicity and cytotoxicity of benz[a]anthracene diol epoxides and tetrahydro-epoxides - exceptional activity of bay region 1,2-epoxides, Proc. Natl. Acad. Sci. 74 (7) (1977) 2746–2750.

[143] K.C. Olson, et al., Characterization of dibenzo[a,l]pyrene-trans-11,12-diol (dibenzo[def,p]chrysene) glucuronidation by UDP-glucuronosyltransferases, Chem. Res Toxicol. 24 (9) (2011) 1549–1559.

[144] I. Janik, G.N.R. Tripathi, The nature of the superoxide radical anion in water, J. Chem. Phys. 139 (1) (2013).

[145] M. Thafar, et al., Comparison study of computational prediction tools for drug-target binding affinities, Front. Chem. 7 (2019) 782.

[146] C. Czajkowski, C. Kaufmann, A. Karlin, Negatively charged amino-acid-residues in the nicotinic receptor delta-subunit that contribute to the binding of acetylcholine, Proc. Natl. Acad. Sci. 90 (13) (1993) 6285–6289.

[147] O. Lockridge, D.M. Quinn, Substrate Molecular Recognition, in: C.A. McQueen (Ed.), Comprehensive Toxicology, Elsevier, 2010.

[148] W.G. Zhong, et al., From ab initio quantum mechanics to molecular neurobiology: a cation-pi binding site in the nicotinic receptor, Proc. Natl. Acad. Sci. 95 (21) (1998) 12088–12093.

[149] I. Denya, S.F. Malan, J. Joubert, Cholinesterases: Isoforms and Function, in: P. Grunwald (Ed.), in *Pharmaceutical Biocatalysis. Fundamentals, Enzyme Inhibitors, and Enzymes in Health and Diseases*, Jenny Stanford Publishing, 2019, p. 428.

[150] J.B. Cohen, S.D. Sharp, W.S. Liu, Structure of the agonist-binding site of the nicotinic acetylcholine-receptor. [3H] acetylcholine mustard identifies residues in the cation-binding subsite, J. Biol. Chem. 266 (34) (1991) 23354–23364.

[151] J. Clayden, et al., Aromatic heterocycles 1: structures and reactions. in Organic Chemistry, Oxford,, 2001, p. 1149.

[152] Hans Reich's Collection. Bordwell pKa Table.

[153] M. Tantama, S. Licht, Use of calculated cation-π binding energies to predict relative strengths of nicotinic acetylcholine receptor agonists, ACS Chem. Biol. 3 (11) (2008) 693–702.

[154] H.M. Guo, et al., Synthesis and evaluation of a cyclic imine derivative conjugated to a fluorescent molecule for labeling of proteins, Bioorg. Med. Chem. Lett. 19 (4) (2009) 1210–1213.

[155] *toxins such as toxiferine, caulerpicin, strychnine and apparicine.*

[156] S. Lee, J. Sperry, Isolation and biological activity of azocine and azocane alkaloids, Bioorg. Med. Chem. 54 (2022), 116560.

[157] M. Boujut, et al., Indazole versus indole-based cationic merocyanines with red shifted in-cellulo emission for selective mitochondria imaging, Dyes Pigments 198 (2022), 109988.

[158] N. Halder, G. Lal, Cholinergic system and its therapeutic importance in inflammation and autoimmunity, Front. Immunol. 12 (2021), 660342.

[159] M. Skok, Mitochondrial nicotinic acetylcholine receptors: mechanisms of functioning and biological significance, Int. J. Biochem. Cell Biol. 143 (2022), 106138.

[160] C.N.S. Breda, et al., Mitochondria as central hub of the immune system, Redox Biol. 26 (2019), 101255.

[161] E.K. Wujcik, et al., An acetylcholinesterase-inspired biomimetic toxicity sensor, Chemosphere 91 (8) (2013) 1176–1182.

[162] J. Misik, et al., Cholinesterase Inhibitor 6-Chlorotacrine - in vivo toxicological profile and behavioural effects, Curr. Alzheimer Res. 15 (6) (2018) 552–560.

[163] S.L. Murov. Toxicity of Substances 7/19/2017 ⟨http://murov.info/toxexe.htm⟩.

[164] J.P.M. Vink, The origin of speciation: trace metal kinetics over natural water/ sediment interfaces and the consequences for bioaccumulation, Environ. Pollut. 157 (2) (2009) 519–527.

[165] K. Heye, et al., Laboratory-to-field extrapolation: increase in carbamazepine toxicity in a higher tier, multiple-stress experiment, Ecotoxicol. Environ. Saf. 183 (2019).

[166] K. Heye, et al., Interactive effects of biotic and abiotic environmental stressors on carbamazepine toxicity in the non-biting midge Chironomus riparius, Water Res. 156 (2019) 92–101.

[167] D. De Zwart, L. Posthuma, Complex mixture toxicity for single and multiple species: proposed methodologies, Environ. Toxicol. Chem. 24 (10) (2005) 2665–2676.

[168] S. Karmakar, et al., Beverage-induced enhanced bioavailability of carbamazepine and its consequent effect on antiepileptic activity and toxicity, J. Food Drug Anal. 23 (2) (2015) 327–334.

[169] B. Croissant, et al., Oxcarbazepine in rapid benzodiazepine detoxification, Am. J. Drug Alcohol Abus. 34 (5) (2008) 534–540.